

# Metabolic remodeling in tumor-associated macrophages contributing to antitumor activity of cryptotanshinone by regulating TRAF6-ASK1 axis

Jia-Hau Yen,<sup>1,15</sup> Wei-Chieh Huang,<sup>2,3,15</sup> Shu-Ching Lin,<sup>1</sup> Yi-Wen Huang,<sup>1</sup> Wan-Ting Chio,<sup>1</sup> Gregory J. Tsay,<sup>4,5,6</sup> Mien-Chie Hung,<sup>7,8,9,10,11</sup> and Sheng-Teng Huang<sup>1,12,13,14</sup>

<sup>1</sup>Research Cancer Center for Traditional Chinese Medicine, Department of Medical Research, China Medical University Hospital, Taichung, Taiwan; <sup>2</sup>Graduate Institute of Integrated Medicine, China Medical University, Taichung, Taiwan; <sup>3</sup>Chinese Medicine Research Center, China Medical University, Taichung, Taiwan; <sup>4</sup>Research and Development Center for Immunology, China Medical University, Taichung, Taiwan; <sup>5</sup>Division of Immunology and Rheumatology, Department of Internal Medicine, China Medical University Hospital, Taichung, Taiwan; <sup>6</sup>School of Medicine, College of Medicine, China Medical University, Taichung, Taiwan; <sup>7</sup>Research Center for Cancer Biology, China Medical University, Taichung, Taiwan; <sup>8</sup>New Drug Development Center, China Medical University, Taichung, Taiwan; <sup>9</sup>Center for Molecular Medicine, China Medical University Hospital, Taichung, Taiwan; <sup>10</sup>Graduate Institute of Biomedical Sciences, Research Center for Cancer Biology and Center for Molecular Medicine, China Medical University Taichung, 100, Sec. 1, Jingmao Road, Beitun District, Taichung 406, Taiwan; <sup>11</sup>Department of Biotechnology, Asia University, Taichung, Taiwan; <sup>12</sup>Department of Chinese Medicine, China Medical University Hospital, No. 2, Yude Road, North District, Taichung 40447, Taiwan; <sup>13</sup>School of Chinese Medicine, China Medical University, No. 2, Yude Road, North District 40447, Taichung, Taiwan; <sup>14</sup>An-Nan Hospital, China Medical University, Tainan, Taiwan

**Dampening tumor growth by converting tumor-associated macrophages (TAMs) from M2/repair-types to M1/kill-types is of high interest. Here, we show that cryptotanshinone (CPT) can function as an antitumor immune modulator that switches TAMs from an M2 to an M1 phenotype, leading to tumor regression. An orthotopic triple-negative breast cancer (TNBC) implantation model was used to determine the role and mechanism of CPT in suppressing M1-to-M2 repolarization of TAMs. Co-culturing TNBC cells with CPT-treated macrophages reduced TNBC proliferation and motility, while in TNBC orthotopic mouse models, CPT treatment inhibited breast tumor formation.**

**Moreover, we identified that CPT inhibits mitochondrial oxidative phosphorylation and mitochondrial fusion via autophagy and transcriptional activation of the apoptosis signal-regulating kinase 1 (ASK1) pathway. Suppression of ASK1 downregulates autophagy and abolishes CPT-induced effects upon TAMs. In addition, CPT inhibits M2 macrophage differentiation and causes TRAF6 auto-ubiquitination-dependent activation of the ASK1, leading to M1 polarization. On the contrary, in M1 macrophage, CPT increases interaction of ASK1 and TRAF6 which induces ASK1 ubiquitination and degradation. Intriguingly, CPT plays opposite roles in the M1 and M2 phenotype. Our findings help to illuminate a previously unrecognized antitumor mechanism of CPT and suggest that this natural compound offers a macrophage-based approach for cancer immunotherapy.**

## INTRODUCTION

Macrophage recruitment and proinflammatory differentiation play critical roles in innate immunity, including antitumor activity.

From their inception, tumors are intimately involved with the immune system. Macrophages that infiltrate tumor tissues or are polarized in the tumor microenvironment (TME) of malignant tumors are defined as tumor-associated macrophages (TAMs),<sup>1-3</sup> which are among the most abundant types of host immune cells in the TME.<sup>4</sup> Increased numbers and/or densities of TAMs correlate unequivocally with poor prognosis.<sup>5</sup> Substantial evidence indicates that TAMs, rather than being only tumoricidal, can adapt and promote tumorigenesis, as well as metastasis. Thus, targeting TAMs is regarded as a promising strategy in cancer immunotherapy.<sup>6</sup>

TAMs are generally thought to contain M2/repair-like phenotypes that enhance cancer progression, although the phenotypes and exact roles of TAMs are under contention.<sup>7,8</sup> Research has identified M1/kill-like TAMs that trigger inflammation and direct T cells toward T helper 1 (Th1) tumoricidal responses,<sup>7,8</sup> revealing that TAMs possess a remarkable degree of plasticity and functional heterogeneity. At tumor initiation, macrophages create immune-activated inflammatory responses that contribute to the mutagenic stress faced

Received 8 October 2021; accepted 17 June 2022;  
<https://doi.org/10.1016/j.omto.2022.06.008>.

<sup>15</sup>These authors contributed equally

**Correspondence:** Mien-Chie Hung, Graduate Institute of Biomedical Sciences, Research Center for Cancer Biology and Center for Molecular Medicine, China Medical University, 100, Sec. 1, Jingmao Road, Beitun District, Taichung 406, Taiwan.

**E-mail:** [mhung@cmu.edu.tw](mailto:mhung@cmu.edu.tw)

**Correspondence:** Sheng-Teng Huang, School of Chinese Medicine, China Medical University; Department of Chinese Medicine, China Medical University Hospital, No. 2, Yude Road, North District, Taichung 40447, Taiwan.

**E-mail:** [sheng.teng@yahoo.com](mailto:sheng.teng@yahoo.com); [d98294@mail.cmuh.org.tw](mailto:d98294@mail.cmuh.org.tw)



by cancer cells. During this transition from a state of benign growth to one that facilitates invasive cell proliferation, the microenvironment appears to be dominated by cytokines and growth factors that facilitate a conversion from this Th1-like inflammatory response toward a Th2-type immune environment. In a mouse model of breast cancer, the change in state from cytotoxic to supportive occurs through the recruitment of interleukin (IL)-4 secreted CD4<sup>+</sup> T cells to the tumor via an unidentified mechanism.<sup>9,10</sup> T cell surface presentation of programmed death-ligand 1 (PD-L1) and B7-homologs activate programmed cell death protein 1 (PD-1) and cytotoxic T-lymphocyte antigen 4 (CTLA-4),<sup>11</sup> respectively, enabling TAMs to directly reduce CD4<sup>+</sup> T cell proliferation and Th1 cytokine production, further inhibiting CD8<sup>+</sup> T cell cytolytic functioning. The transition to malignancy is also exacerbated by TAMs through their secretion of vascular endothelial growth factor A (VEGF-A) and angiogenic factors CXCL8 and CXCL12, as well as production of proteases (cysteine cathepsin proteases, serine proteases, neutrophil elastase, and proteinase 3 [P3]).<sup>12–14</sup> Specific metabolic cascades are increasingly recognized as critical hallmarks of macrophage subsets.<sup>15</sup> M2 cells display an intact tricarboxylic acid (TCA) cycle and functional mitochondrial oxidative phosphorylation (OXPHOS)<sup>16</sup> with impairment of inducible nitric oxide synthase (iNOS) generation of NO from L-arginine and inhibiting glycolysis for rapid pathogen killing.<sup>17</sup> Thus, targeting M2-like TAMs and depleting them in the TME or reprogramming M2-like TAMs into M1-like phenotypes, which directly boosts their tumoricidal activities and indirectly stimulates cytotoxic T cells to eliminate tumor cells, is a potential strategy for cancer immunotherapy.

Cryptotanshinone (CPT), a natural quinoid diterpene isolated from the herb *Salvia miltiorrhiza* (Danshen), inhibits the activation of signal transducer and activator of transcription 3 (STAT3).<sup>18</sup> Furthermore, CPT has demonstrated promising pharmacological activity in cardiovascular disease by inhibiting tumor necrosis factor alpha (TNF- $\alpha$ )-induced early atherogenic events *in vitro*,<sup>19</sup> by suppressing the secretion of inflammatory cytokines in RAW 264.7 macrophages,<sup>20</sup> and by protecting primary rat cortical neurons from glutamate-induced neurotoxicity.<sup>21</sup> CPT displays diverse anticancer activity in humans, including prostate cancer, leukemia, gliomas, lung carcinomas, hepatic carcinomas, pancreatic cancer, breast cancer, colorectal cancer, and melanoma.<sup>22–27</sup> Mechanistically, its antitumor effect has been ascribed to the direct targeting of tumor cells and/or tumor-derived endothelial cells. The broad antitumor activities raise an interesting possibility as whether CPT might associate with macrophage-modifying activity to contribute to antitumor activity. Indeed, in the current study, we reveal that CPT functions as a novel macrophage-based tumor immunotherapy and mediating its antitumor efficacy by reprogramming TAMs from M2-to-M1 phenotypes.

## RESULTS

### CPT-mediated inhibition of orthotopic TNBC growth is macrophage-dependent

To address whether macrophages may be involved in CPT-mediated antitumor effects, we treated mice with clodronate liposomes to deplete macrophages<sup>28</sup> (Figure 1A). Using MDA-MB-231 tumor-

bearing mice, we found that CPT effectively inhibited tumor growth, while tumors relapsed in mice with a depleted macrophage population (Figures 1B–1D). We found that macrophage depletion disrupted the inhibitory effect of CPT on triple-negative breast cancer (TNBC) growth. The numbers of inflammatory monocytes in bone marrow or the circulating system of CPT-treated mice did not change significantly (Figure 1E). We confirmed that macrophage removal disrupted the inhibitory effect of CPT on TNBC growth. Macrophages consist of two main subsets: the proinflammatory M1 (CD80<sup>+</sup>, iNOS<sup>+</sup>, mannose receptor [MR]<sup>-</sup>) and the anti-inflammatory M2 (MR<sup>+</sup>, CD80<sup>-</sup>, iNOS<sup>-</sup>) subset, which is abundantly present in the TME and essentially plays a critical role in coordination with tumor cells. To clarify the effects of CPT upon TME profiling, tissue immunofluorescence results demonstrate that CPT treatment increased iNOS expression but decreased MR expression, an M2 macrophage marker (Figure 1F). Thus, CPT-mediated macrophage polarization may contribute to its antitumor responses in TNBC.

### CPT treatment blunts mitochondrial oxidative respiration in macrophages

Metabolic cascades are known to exhibit particular characteristics (such as the pentose phosphate pathway and the TCA cycle) and metabolic shifts that fuel multiple aspects of activation. During inflammatory stimuli, macrophages switch from OXPHOS to glycolysis as their main source of energy.<sup>29–31</sup> Preventing these shifts impairs the activation of macrophages. To investigate how CPT may induce macrophage polarization to contribute to anticancer activity, we studied the effect of CPT on macrophage metabolism. RAW 264.7 cells were induced to obtain M1 and M2 population of macrophages with appropriate reagents,<sup>32,33</sup> then treated with or without CPT. The RNA from these cells was subjected for RNA sequencing (RNA-seq) analysis (Figure 2A). Hierarchical clustering of the RNA-seq dataset allowed us to identify 139 genes that were downregulated and 206 genes that were upregulated by CPT treatment in RAW 264.7 macrophages under M1 conditions. When the macrophages were subjected to M2 conditions, CPT downregulated 18 genes and upregulated 54 genes (Figure S1). Pathway analyses of CPT-regulated genes identified several processes known to be regulated by the immune response, such as nuclear factor kappa B (NF- $\kappa$ B) and cytokine signaling, but also several metabolic pathways that have not previously been identified as having any involvement with macrophages (Figure 2B). When assessing the viability of differentially stimulated macrophages, we observed that M1 and especially M2 macrophages were less active than naive macrophages in the MTT assay (Figure 2C). However, a similar percentage of annexin V<sup>-</sup> propidium iodide<sup>-</sup> living cells showed no statistical changes under all test conditions (Figure 2D). Since mitochondrial dehydrogenase activity is the primary target of MTT, these controversial results suggested that the lower MTT observation was due to metabolic differences in these macrophages. This prompted us to assess the metabolic characteristics of polarized macrophages by metabolic flux analysis, especially on account of recent evidence revealing that metabolic reprogramming controls macrophage

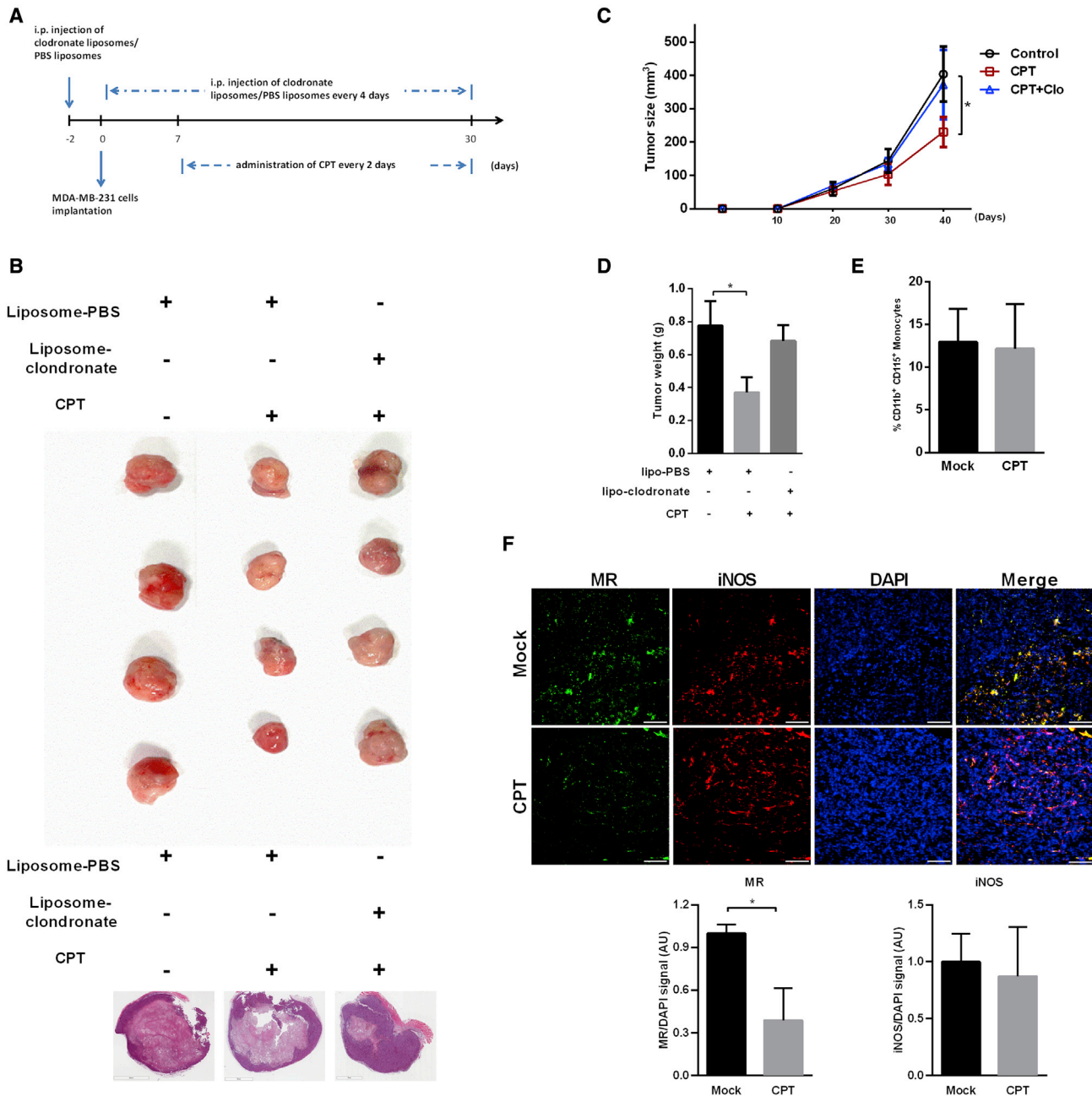
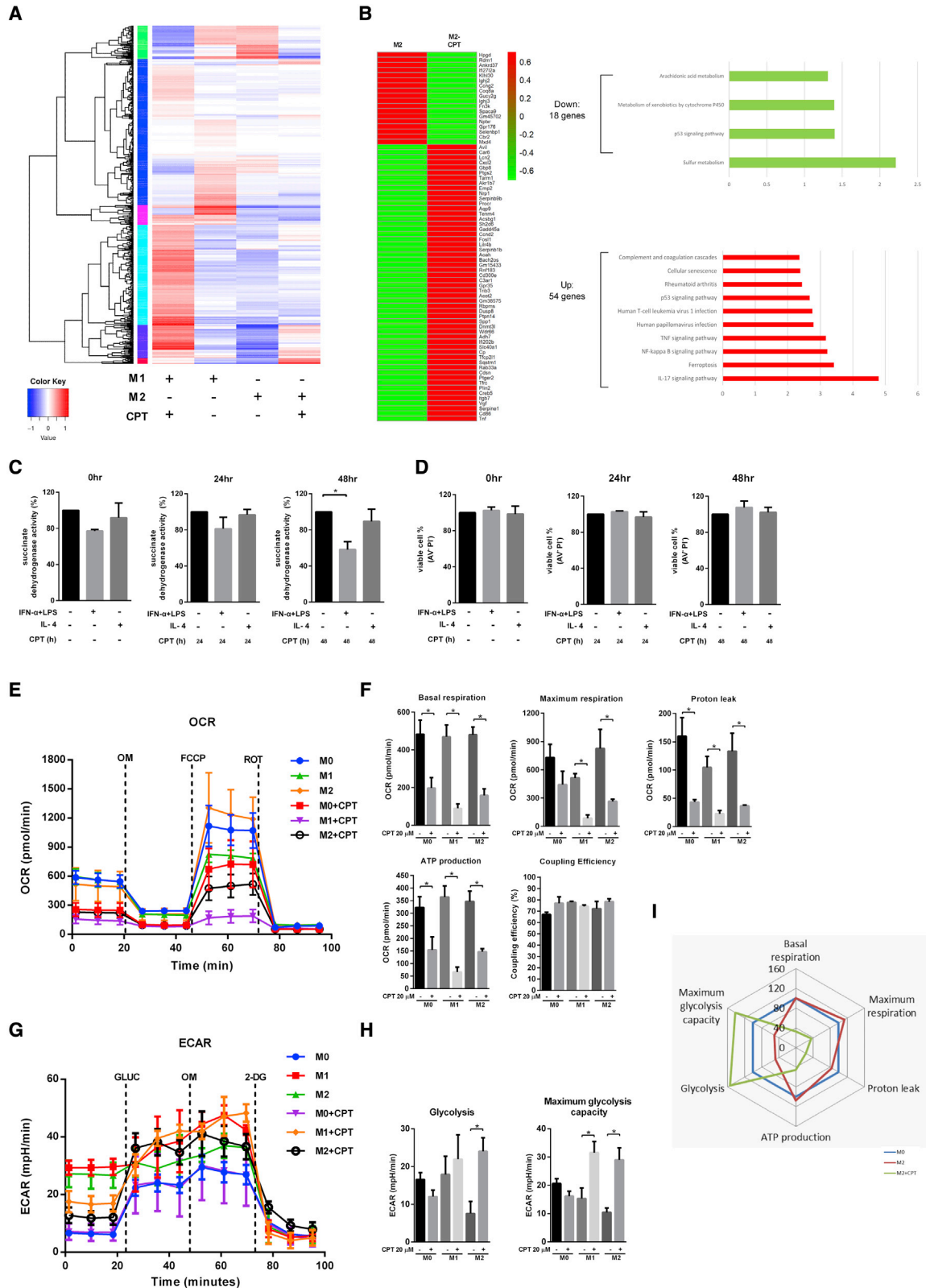


**Figure 1. Inhibition of orthotopic TNBC growth by CPT requires the presence of macrophages**

(A) Schematic presentation of the experimental procedure. (B) Removal of macrophages from mice prevented the antitumor effects of CPT. Orthotopic TNBC tumor growth was significantly inhibited in CPT-treated mice, whereas removal of macrophages by intraperitoneal injections of clodronate liposome led to breast tumor recurrence. Representative micrographs of H&E staining and tumor images are shown. (C and D) MDA-MB-231 cell-derived tumors were developed in SCID mice and treated with vehicle or CPT. Tumor growth was monitored by tumor volume and tumor weight for 4 weeks ( $n = 10$  mice/group;  $*p < 0.05$ ). (E) CPT treatment did not elevate monocyte populations in the circulation system. (F) CPT treatment was associated with increases in M1 markers and reduced M2 populations. Antibodies against iNOS (M1 marker) and the mannose receptor (MR, an M2 marker) were used to stain frozen sections of breast tissue.

activation and function.<sup>30</sup> It has been established that M1 macrophages use glycolysis, whereas M2 macrophages are biased toward oxidative phosphorylation. In line with this observation, we found

that CPT treatment significantly decreased the basal and maximum oxygen consumption rates (OCR) (Figures 2E and 2F). Glycolysis characteristics were calculated from the changes in extracellular



(legend on next page)

acidification rate (ECAR) in response to glucose, oligomycin (OM), and 2-deoxyglucose (2-DG) injection. We confirmed that CPT treatment increased basal extracellular acidification rates (ECAR) in interferon (IFN)- $\gamma$  + lipopolysaccharide (LPS)-conditioned M1 and IL-4-conditioned M2 macrophages, which could be further enhanced by the addition of OM and subsequent inhibition of mitochondrial oxidative phosphorylation (Figures 2G and 2H). As shown in Figure 2I, we determined that all calculated metabolic parameters in CPT-treated M2 macrophages exhibited reprogramming toward glycolysis, suggesting that CPT is capable of promoting anaerobic glycolysis in M2 macrophages.

### CPT resets the phenotype of tumor-associated M2 macrophages to the M1 phenotype and ameliorates tumor proliferation

Next, we investigated how CPT regulates macrophage activity and suppresses tumor growth. The classical activation of macrophages (M1) occurs following challenge of pathogen-associated molecular patterns, leading to the upregulation of costimulatory molecules and conferring on them the ability to kill tumor cells by producing NO and TNF- $\alpha$ , or by using other means such as phagocytosis.<sup>10</sup> We found that CPT-mediated transcriptional upregulation of *CXCL2*, *TRIB3*, prostaglandin E receptor 2 (PTGER2), and *CD86* occurred simultaneously with the downregulation of several metabolism pathways (Figure 2B). CPT-treated TAMs consistently expressed higher levels of CD86 and CD80 (M1 markers), whereas CD206 (M2 marker) levels were largely decreased in a dose-dependent manner (Figure 3A). When we checked the effect of CPT on mitochondria morphology via MitoTracker Green FM, we found that CPT caused mitochondria fission both before and after IL-4 treatment (Figure 3B). In addition, CPT-treated macrophages produced higher levels of both whole-cell (total) NO and mitochondrial reactive oxygen species (ROS) in response to M2 conditions (Figure 3C). Accordingly, CPT treatment increased the transcription of nitric oxide synthase 2 (*Nos2*) in M2, but not M1 macrophages (Figures 3D and 3E). We hypothesized that reprogramming toward M1 macrophages in response to CPT leads to tumoricidal activity. To test this hypothesis, MDA-MB-231 cells were co-cultured for 48 h with TAMs pretreated with vehicle or 20  $\mu$ M CPT for 48 h. Co-culturing of CPT-pretreated TAMs with MDA-MB-231 cells suppressed the motility of TNBC cells (Figures 3F and 3G). Furthermore, co-culturing of CPT-pretreated TAMs inhibited TNBC cell proliferation (Figure 3H). These findings indicate that CPT suppressed tu-

mor cell expansion by initiating direct reprogramming effects on polarized macrophages.

### CPT resets tumor-associated M2 macrophages to the M1 phenotype

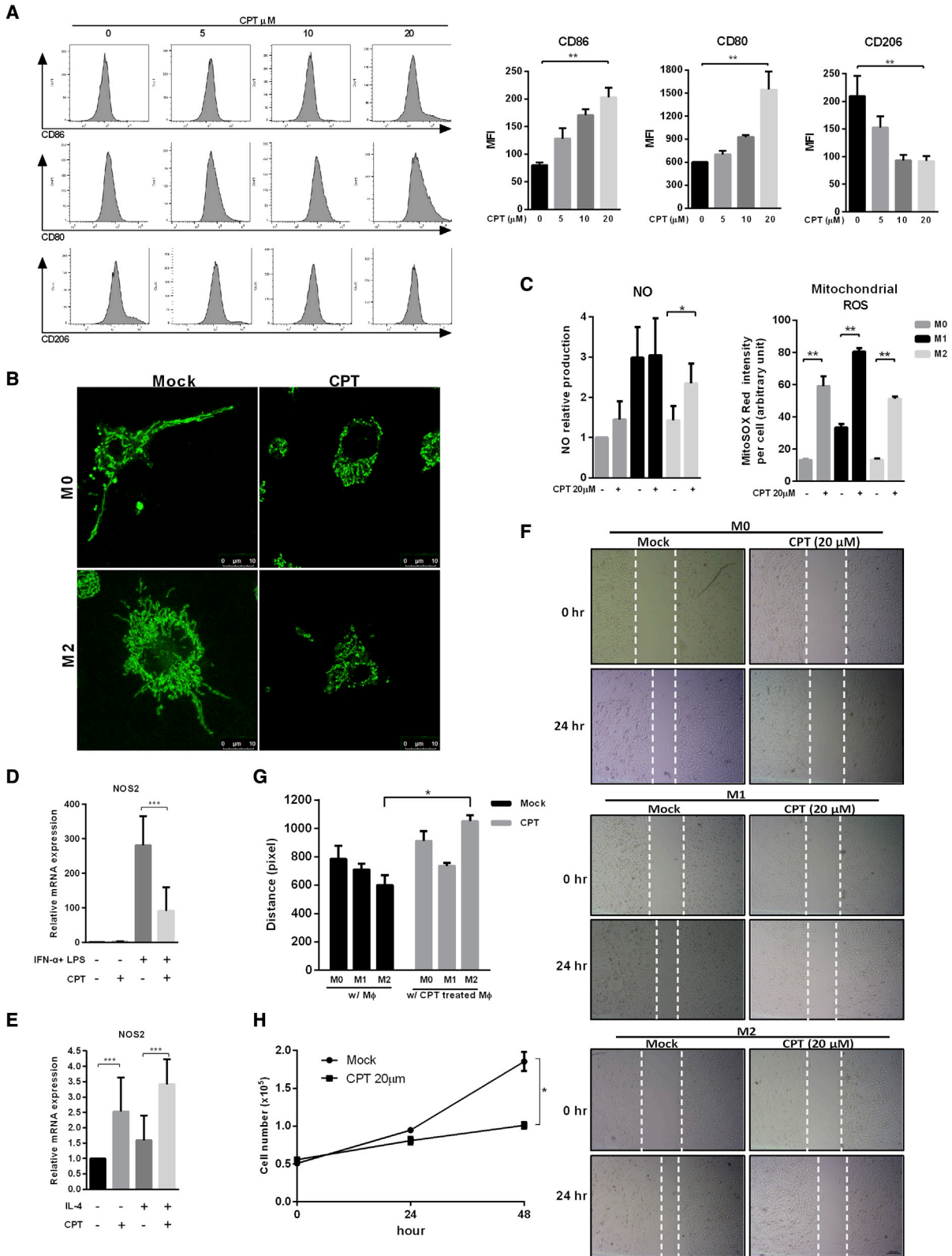
M1 macrophages produce proinflammatory cytokines (IL-12, NO, etc.) that inhibit tumor cell growth, while the M2 phenotype secretes a series of protumoral factors (IL-10, arginase 1, etc.) that promote tumor expansion.<sup>32,33</sup> To investigate how CPT regulates macrophages toward the M1 phenotype and induces tumor suppression, we examined cytokine expression profiles in CPT-treated macrophages. Consistent with the phenotypic analysis, we observed upregulation of the proinflammatory genes, *IL-6*, *IL-12A*, and *IL-12B* in CPT-treated M1 macrophages and downregulation of the anti-inflammatory gene, *IL-10* (Figure 4A). Transcription of *IL-1 $\beta$*  was decreased but *TNF- $\alpha$*  remained unchanged. In IL-4-activated macrophages, CPT-treated macrophages expressed higher levels of several genes encoding proinflammatory cytokines, including *TNF- $\alpha$* , *IL-12A*, and *IL-12B*, whereas expression of *IL-1 $\beta$*  and *IL-10* was decreased (Figure 4B). At the same time, cytokine protein expression, including IL-1 $\beta$ , IL-6, and TNF- $\alpha$ , was higher in CPT-treated IL-4 treated RAW 264.7 cells, while IL-10 protein was lower in both CPT-treated IFN- $\alpha$ +LPS and IL-4-activated RAW 264.7 cells (Figures 4C and 4D). Exposure of bone marrow-derived macrophages (BMDMs) to CPT also induced the secretion of the proinflammatory cytokines IL-1 $\beta$ , IL-6, and TNF- $\alpha$  in response to IL-4 stimulation, whereas this did not occur with LPS + IFN- $\gamma$  in BMDMs (Figures 4E and 4F). The results of IL-12A and IL-12B were also confirmed by immunoblotting (Figure S2). These results demonstrate that increased production of proinflammatory cytokines in CPT-treated macrophages is critical for tumoricidal activity.

### Induction of autophagy is involved in repolarization of CPT-treated TAMs

Our recent study described how CPT behaved as a natural autophagy inducer in cancer cells,<sup>24</sup> while previous research has reported that the JAK/STAT signaling pathway regulates autophagy.<sup>34</sup> Thus, we explored whether the JAK/STAT pathway regulates autophagy associated with macrophage reprogramming. Similar to our previous findings, we observed that CPT is an efficient STAT3 inhibitor (Figure 5A). After 48 h of CPT treatment, p-STAT6 was downregulated in M1 cells. Tumor necrosis factor receptor-associated factor 6 (TRAF6) was upregulated in CPT-treated M1 macrophages, but downregulated in the M2 condition. Consistently, we observed a decrease in the LC3-II/LC3-I

### Figure 2. CPT reprograms macrophage metabolism

(A) A heatmap showing baseline gene expression in CPT-treated M1 and M2 BMDMs. (B) Hierarchical clustering and an expression heatmap of CPT-regulated genes in M2 BMDMs with or without 20  $\mu$ M of CPT treatment for 24 h, as determined by RNA-seq. (C) An MTT assay measured mitochondrial succinate dehydrogenase activity. (D) RAW 264.7 cells were subjected to Annexin V plus 7-AAD staining to determine the percentage of viable cells. (E) Oxygen consumption rates (OCR) of M0, M1, and M2 RAW 264.7 cells were measured with or without 20  $\mu$ M of CPT treatment for 24 h ( $n = 3$  in each group). (F) Bar graphs show OXPHOS parameters derived from OCR values. (G) Extracellular acidification rate (ECAR) of M0, M1, and M2 RAW 264.7 cells that were untreated or exposed to CPT for 24 h ( $n = 3$  in each group). (H) Bar graphs show glycolysis parameters from ECAR values. (I) All calculated metabolic parameters in M2 and CPT-treated M2 cells are shown relative to those in naive M0 macrophages ( $N = 100\%$ ) with radar scheme. The results are expressed as the means  $\pm$  SD from three independent experiments. \* $p < 0.05$  compared with controls.



(legend on next page)

ratio in CPT-treated M1 macrophages. It should be noted, however, that the ratio was increased upon CPT treatment in M2 macrophages and was accompanied by modest increases in ATG5 expression and decreases in phospho-mTOR compared with the M1 condition. Although phospho-JNK was upregulated in response to CPT in M0 and M2 macrophages, but not in M1 macrophages, we speculated that induction of autophagy by CPT could only be achieved in unpolarized and M2 macrophages, not in M1 macrophages. To prove this hypothesis, we used bafilomycin A1 and RNA interference (RNAi) against the *ATG5* gene to suppress induction of autophagy in M2 macrophages. As shown in Figure 5B, we observed that bafilomycin A1 inhibited autophagosome-lysosome fusion and increased autophagic flux activity induced by CPT. Interestingly, the reprogramming of M2 to M1 phenotypes by CPT was abolished upon ATG5 depletion (Figures 5C and 5D). In line with the macrophage surface markers, ATG5 depletion reversed the changes in expression of proinflammatory cytokines IL-1 $\beta$ , IL-6, and TNF- $\alpha$  induced by CPT in both RAW 264.7 and BMDM cells (Figure 5E). These observations demonstrate that autophagy is involved in CPT-induced resetting of TAM phenotypes.

#### Autophagy-associated activation of the ASK1 pathway mediates CPT-induced repolarization of TAMs

Inspection of the raw RNA-seq data revealed a significantly higher signal of TNF- signaling and its dependence on the ASK1 signaling pathway.<sup>35,36</sup> In order to confirm this outcome, we examined the expression of ASK1 and TAB family proteins. Increased levels of ASK1 and transforming growth factor  $\beta$ -activated protein kinase 1 (TAK1)-binding protein-1, -2, -3 (TAB1, 2, 3) revealed activation of cellular responses to TNF receptor-1 (TNFR1) in CPT-treated TAMs (Figure 6A). To further clarify the role of ASK1 in macrophage polarization, we quantified levels of ASK1 expression in M1 or M2 macrophages treated with or without CPT. We found that ASK1 was upregulated in M1 macrophages and that this was blocked by CPT treatment (Figure 6B). The opposite effects were seen with CPT treatment in M2 RAW 264.7 cells and BMDMs (Figure 6B). In a time course experiment, we observed initial increases in ASK1 expression that subsequently decreased in M1 macrophages and increased in M2 macrophages, in time-dependent manners (Figure 6C). Recent studies report that ASK1 mediates cytokines and oxidative stress (ROS) in a mitochondria-dependent pathway.<sup>37</sup> We observed that CPT upregulated ASK1 in both cytosol and mitochondria (Figure 6D). To determine whether ASK1 is involved in CPT-

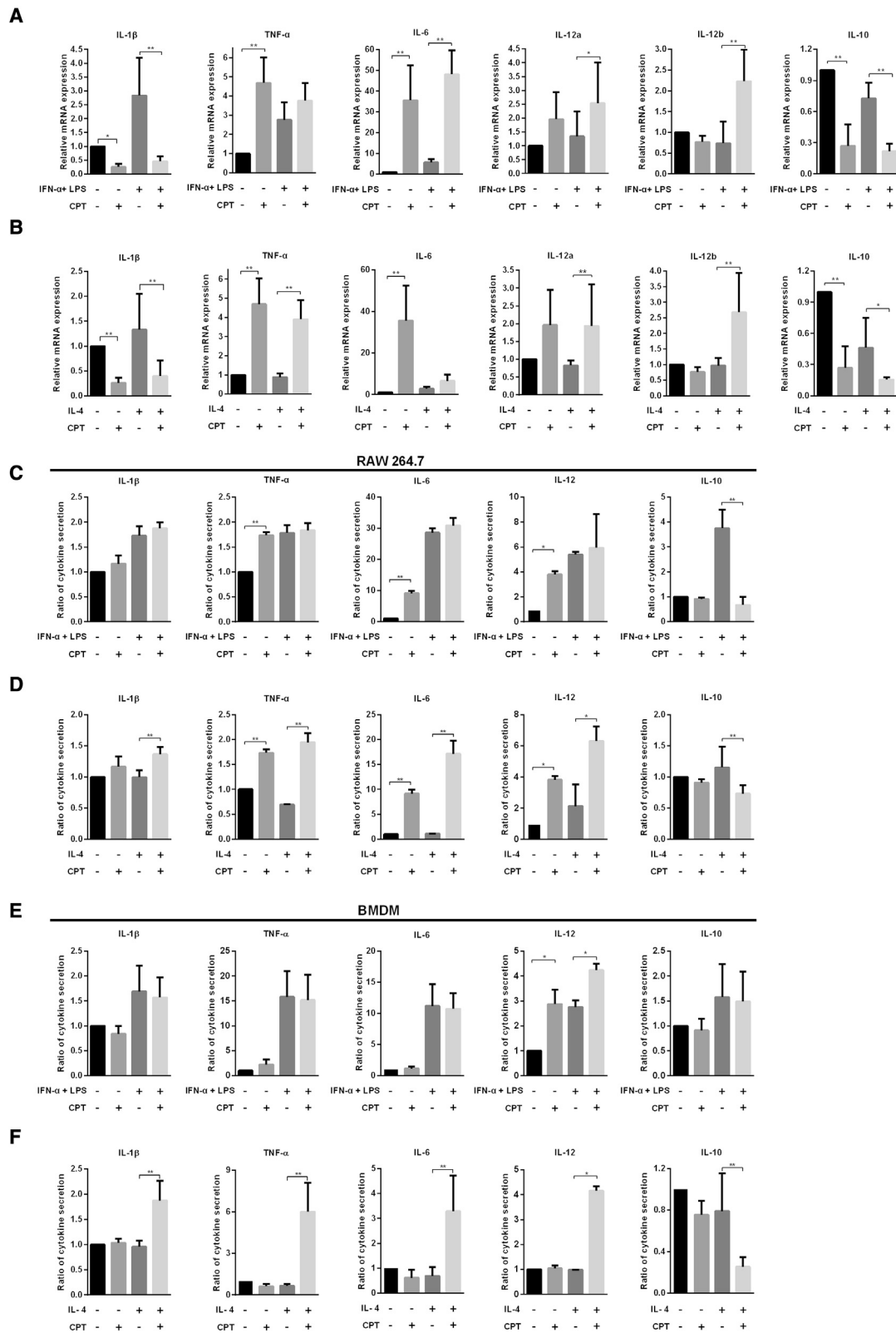
induced autophagy, we evaluated the effect of RNAi against the *ASK1* gene. As shown in Figure 6E, silencing of *ASK1* in CPT-treated M2 macrophages prevented the induction of p-JNK and LC3-II. Inhibition of *ASK1* by RNAi and NQD1 (an *ASK1* inhibitor) and silencing of *ASK1* restored M2 phenotypic characteristics in CPT-treated cell OCR values (Figures 6F and 6G). Silencing of *ASK1* by NQD1 as well as selonsertib (an *ASK1* inhibitor) significantly decreased the levels of expression of proinflammatory cytokines IL-1 $\beta$ , IL-6, TNF- $\alpha$ , and NO in RAW 264.7 cells and BMDMs (Figures 6H and S3). The high expression of *ASK1* in M1 macrophages, but not in unpolarized and M2 macrophages, further confirmed the role of *ASK1* in mediating M2 repolarization induced by CPT.

#### CPT initiates auto-ubiquitination of TRAF6 in M2 macrophages

TRAF6 is an ubiquitin E3 ligase that regulates important biological processes.<sup>38</sup> LPS-induced production of intracellular ROS is required for the formation of a complex consisting of TRAF6 and ASK1.<sup>39</sup> As shown in Figure 7A, CPT enhanced TRAF6 expression in M1 macrophages and suppressed TRAF6 in TAMs; the downregulation in TRAF6 expression occurred in a time-dependent manner in TAMs (Figure 7A); no such effect was seen in M1 macrophages (Figure 5A). This inhibitory effect of CPT on TRAF6 in TAMs was completely abolished in the presence of pharmacological inhibitors of autophagy bafilomycin A1 or knockdown of ATG5 (Figure 7B). Gradual upregulation of TRAF6 was detected when TAMs were co-treated with CPT and bafilomycin A1 (Figure 7C), indicating that reduced expression of TRAF6 in CPT-treated TAMs may be independent to transcriptional suppression of TRAF6 itself but dependent on a degradation pathway. As an E3 enzyme, TRAF6 enables the binding of both E2 and the target molecule, so that ubiquitin can be transferred from E2 to the target protein. Co-immunoprecipitation (co-IP) with TRAF6 antibody in CPT-treated TAMs revealed that immunoprecipitation with TRAF6 was able to pull down ubiquitin (Figure 7D), indicating that CPT markedly promoted TRAF6 ubiquitination. To address the mediatory role of TRAF6 in CPT-induced ASK1 activation in macrophage reprogramming, we performed a parallel experiment using IP TRAF6 to detect its association with ASK1. Interestingly, we observed modest increases in ASK1 in response to interactions with TRAF6 in M1 macrophages, whereas the opposite occurred in M2 macrophages (Figures 7E and 7F). Compared with whole-cell lysates, stronger interactions between TRAF6 and ASK1

#### Figure 3. CPT triggers repolarization of M2e macrophage without impairment in M1 phenotype

(A) CPT treatment skewed TAMs to M1 macrophages. TAMs were induced by culturing BMDM with tumor supernatant (TSN) as described in the [materials and methods](#) section. Cells were subjected to different doses of CPT for 24 h and were stained with antibodies against CD86, CD80, and CD206, then subjected to flow cytometric analysis. The representative histogram represents differentially treated CD11b<sup>+</sup> macrophages, with quantified surface expression values. (B) Comparison of mitochondrial morphology in the control and CPT-treated macrophages. Images of mitochondria (green) were collected by confocal microscope. (C) NO and mitochondrial ROS production were quantified in M0, M1, and M2 RAW 264.7 cells with or without CPT treatment (n = 3 in each group). (D and E) Relative *Nos2* gene expression of RAW 264.7 cells stimulated with LPS + IFN- $\gamma$  (D) or IL-4 (E) with or without CPT 20  $\mu$ M for 24 h. (F) MDA-MB-231 cells were seeded into 24-well cell culture plates and a gap was created by silicone inserts. The cells were then subjected to 24 h of co-culture with polarized macrophages pretreated with vehicle or 20  $\mu$ M CPT for 24 h. MDA-MB-231 cells that were co-cultured with M2 macrophages pretreated with CPT slowly migrated toward the center of the gap. (G) Quantification results in (D). (H) MDA-MB-231 cells were seeded and co-cultured with TAMs pretreated with vehicle or 20  $\mu$ M CPT. Numbers of MDA-MB-231 cells were counted at 24 and 48 h. The proliferation of MDA-MB-231 cells with TAMs pretreated with CPT occurred in a time-dependent manner. The results are expressed as the mean  $\pm$  SD from three independent experiments. \*p < 0.05 compared with controls.



(legend on next page)

downregulated ASK1 in M1 macrophages and BMDMs (Figure 7E), while smaller interactions induced higher ASK1 levels in M2 macrophages and BMDMs (Figure 7F). The results imply that CPT induces TRAF6-dependent ubiquitination of ASK1 and leads to proteasomal degradation in the M1 condition. We therefore examined whether endogenous ASK1 is ubiquitinated in response to CPT. In M1 macrophages, but not in naive and M2 macrophages, the ubiquitination of endogenous ASK1 was increased after CPT treatment, with parallel increases in TRAF6 interaction (Figure 7G). These results indicate that ASK1 co-IP with TRAF6 is ubiquitinated in M1 macrophages treated with CPT and suggest that the CPT-induced activation of TRAF6 E3 ubiquitin ligase mediates its auto-ubiquitination and then protects ASK1 from degradation, which subsequently reprograms M2 macrophages and TAMs toward the M1 state.

## DISCUSSION

TNBC is difficult to treat, but responds to immunotherapy, with cases of relapsed/refractory metastatic TNBC experiencing significant improvements in progression-free and overall survival after treatment with sacituzumab govitecan as compared with single-agent chemotherapy,<sup>40</sup> offering researchers opportunities to test novel strategies that even more effectively harness the immune system and maximize clinical outcomes for patients. Some researchers have focused on ways to deplete M2 TAMs, to block the CCL2/CCR2 recruitment pathway, or to interfere with M2-related signaling pathways such as CD47/SIRP $\alpha$ .<sup>41,42</sup> CPT, a compound purified from *Salvia miltiorrhiza*, is in ongoing research as a potential anticancer therapy. Its anticancer activity is assumed to be mediated by induction of apoptosis in cancer cells via dynamin-related protein 1 (DRP1)-mediated mitochondrial fragmentation.<sup>27</sup> In addition to showing cytotoxic effects in cancer cells, CPT reportedly mediates immune modulation.<sup>19,20</sup> However, it remains to be confirmed as to whether CPT can offer a novel and very effective means of harnessing macrophages to overcome TNBC. In this study, we demonstrate that immune responses govern the antitumor efficacy of CPT and we show that CPT exerts its antitumor effects by reprogramming macrophage function (Figure 7H). Our findings offer an alternative strategy for targeting M2 TAMs.

Divergent metabolism was one of the first defining traits used to distinguish macrophage subsets.<sup>15,43</sup> Resetting the metabolism of the TCA cycle and conversion of arginine to NO through iNOS activity is required for M1 macrophages to efficiently produce proinflammatory effector molecules and provide effective host defense against invading pathogens. Unresolved M1 activation can result in tissue damage and chronic inflammation. Thus, a repair phase is needed, in which M2 cells predominate. As the Yang (M1) or Yin (M2) of macrophage function,<sup>44</sup> M2 cells are low in NO, display high arginase 1 activity, resolve inflammation, and promote tissue repair. The tran-

sition from M1 to M2 can be completed by reprogramming of macrophages and/or replacement of M1 macrophages by recruited monocytes that polarize into M2 in the newly established microenvironment.<sup>44</sup> In support of this notion, converting M2 TAMs into tumor-killing phagocytes has shown enormous promise in cancer therapy.<sup>10,15</sup> Rebalancing macrophage polarization has been described as the “holy grail” of macrophage therapeutic targeting.<sup>45</sup> We found that CPT induces the metabolic characteristics of M1 cells and prevents polarization to an M2 state. Our evidence also revealed that CPT did not increase levels of circulating inflammatory monocytes, indicating that CPT may repolarize local-regional TAMs away from M2 phenotypes. Indeed, in our co-culture study, we observed significant decreased proliferation of TNBC cells when TAMs were pretreated with CPT, which may indicate that production of proapoptotic factors such as TNF- $\alpha$  by CPT-treated TAMs is sufficient to suppress propagation of TNBC cells. According to our evidence, CPT promotes antitumor immunity in a macrophage-dependent manner and we speculate that the downregulation of IL-10 may be a reason for the antitumor effects of CPT.

The key question is how macrophages that are reset by CPT remodel the tumor immune microenvironment, leading to enhanced antitumor immunity. ASK1, which is encoded by MAP3K5, activates the mitogen-activated kinase kinase 4 (MKK4)-JNK, MKK7-JNK, MKK3-p38, and MKK6-p38 pathways, and is essential for cytokine- and stress-induced apoptosis in mammalian cells.<sup>46,47</sup> ASK1 does not activate the NF- $\kappa$ B pathway in mammalian cells.<sup>48</sup> Hence, the ASK1-dependent pathway appears to have an evolutionary precedent other than NF- $\kappa$ B in the host defense system. It was shown recently that ASK1 is needed for regulation of infiltration and activation of macrophages in skin wounds,<sup>49</sup> which implies that ASK1 might be involved in macrophage differentiation. In our experiment, we observed that ASK1 was increased in M1 cells, but decreased in the M2 condition. Unexpectedly, this result was reversed after CPT treatment. A recent study showed that the ASK1/JNK signaling pathway contributes to induction of autophagy. Consistent with these results, Figure 6E showed that CPT-induced JNK activation and autophagy were ASK1 dependent.<sup>50</sup> Genetic and pharmacologic inhibition of ASK1 (by ASK1 deficiency and ASK1 inhibitor treatment) compromises the effects of CPT on downregulation of the OCR and inflammatory cytokines (Figures 6F–6H). These results may interpret that ASK1, a kinase involved in vascular endothelial cell activation and inflammation, is a critical molecule that mediates macrophage repolarization. We found that CPT skews TAMs to the M1 phenotype, without increasing systematic inflammation *in vivo*. Thus, our evidence indicates that CPT exerts antitumor efficacy by regulating immune function. Autophagy has been revealed to play a pivotal role in macrophage population by determining hematopoietic stem cell fate,

### Figure 4. CPT skews M2 macrophage cytokine profiles toward the M1-type

(A and B) Relative gene expression of cytokines of RAW 264.7 cells stimulated with LPS + IFN- $\gamma$  (A) or IL-4 (B) with or without CPT 20  $\mu$ M for 24 h. (C and D) RAW 264.7 cells stimulated with LPS + IFN- $\gamma$  (C) or IL-4 (D) with or without 20  $\mu$ M CPT for 60 h. Secretion of IL-1 $\beta$ , IL-6, TNF- $\alpha$ , IL-10, and IL-12 was measured by ELISA. (E and F) BMDMs stimulated with LPS + IFN- $\gamma$  (E) or IL-4 (F) with or without 20  $\mu$ M CPT for 60 h. Secretion of IL-1 $\beta$ , IL-6, TNF- $\alpha$ , IL-10, and IL-12 was measured by ELISA. The results are expressed as the mean  $\pm$  SD from three independent experiments. \* $p$  < 0.05 and \*\* $p$  < 0.01 compared with controls.

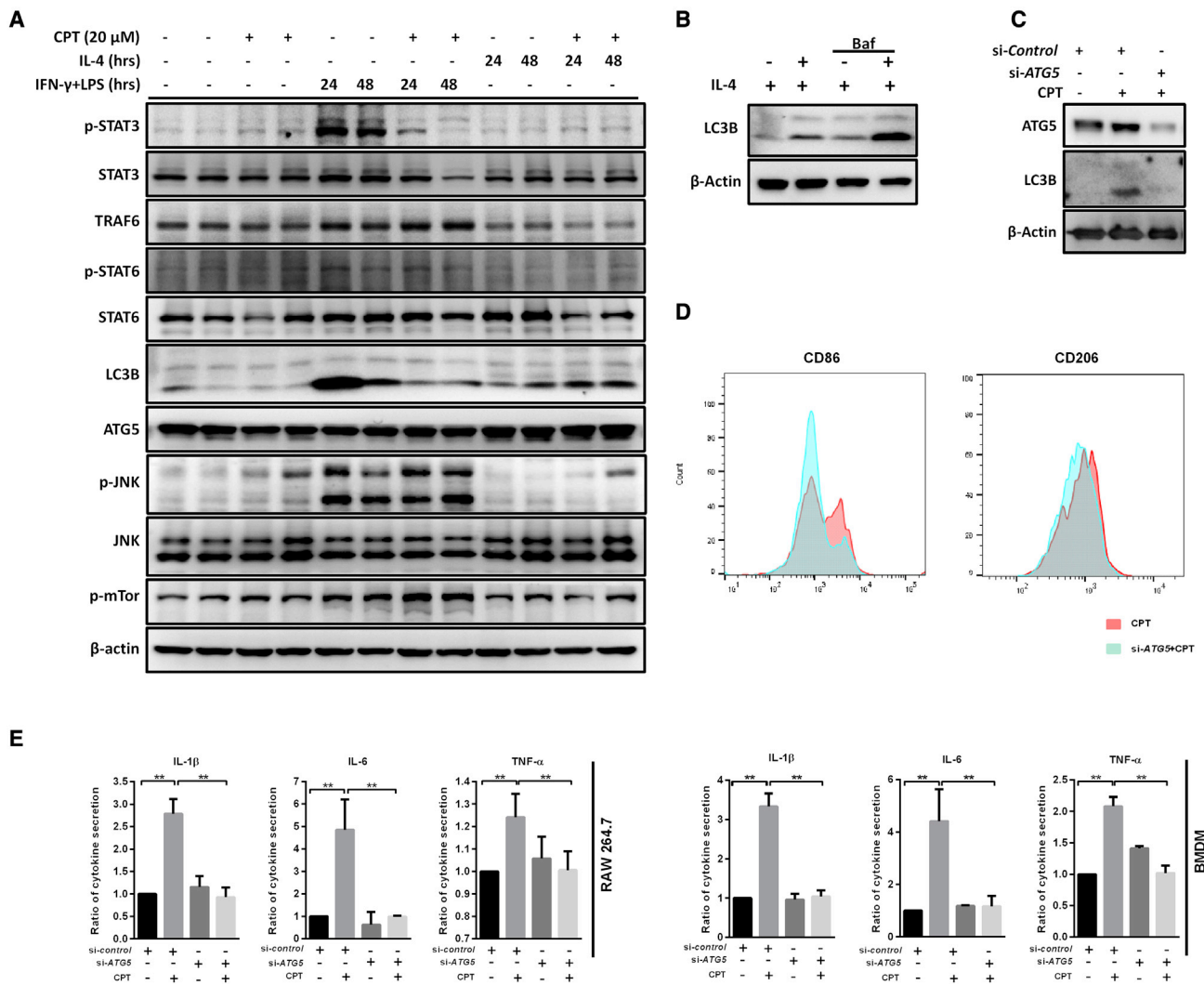


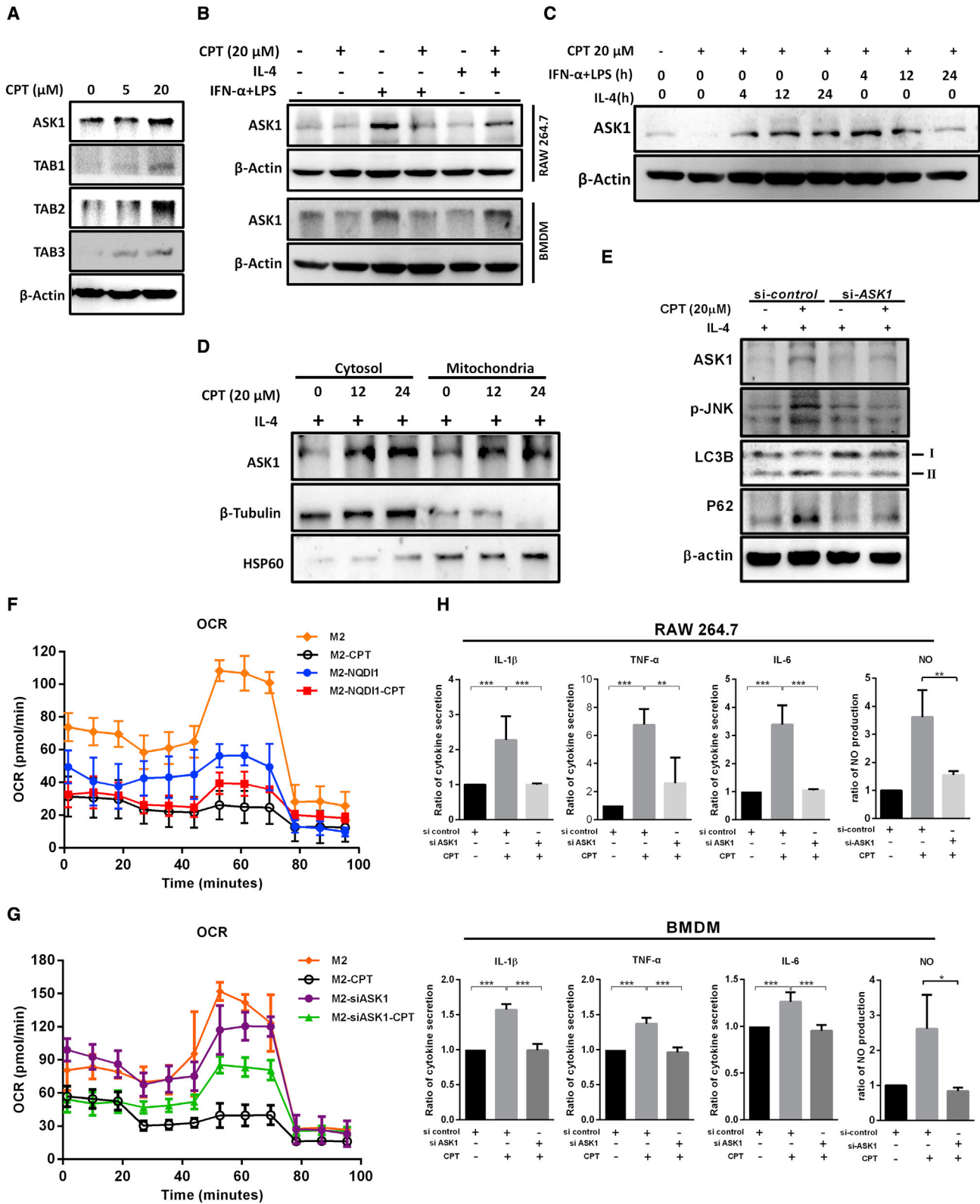
**Figure 5. Induction of autophagy is involved in the repolarization of CPT-treated TAMs**

(A) M1 and M2 conditioned RAW 264.7 cells were treated with or without CPT 20 μM for the indicated times, after which p-STAT3, STAT3, TRAF6, p-STAT6, STAT6, LC3B, ATG5, p-JNK, JNK, and p-mTOR were measured by western blot. β-Actin served as the internal control. (B) M2 conditioned RAW 264.7 cells were pretreated with bafilomycin A1 (3 nM, 2 h) and then co-treated with CPT 20 μM for 24 h. The cells were extracted and LC3B protein levels were assessed by immunoblotting. (C) RNA interference against ATG5 was conducted as described and TAMs were treated with 20 μM CPT for 24 h. ATG5 and LC3B expression was detected by immunoblotting. (D and E) Suppression of ATG5 by RNA interference induced the skewing of CPT-treated TAMs to the M2 phenotype. RNA interference was conducted as described and TAMs were treated with CPT. Suppression of ATG5 expression significantly blocked CPT-induced changes in CD86 expression. This result was supported by observations of the cytokine expression profile (E). The results are expressed as the mean ± SD from three independent experiments. \*\*p < 0.01 compared with controls.

monocyte trafficking, and macrophage differentiation.<sup>51</sup> To further study the physiological relevance of the repolarization activity of CPT associated with autophagy, we sought to examine ATG5 knock-down macrophage of which M1 phenotypic markers were decreased compared with control cells. In line with this concept, we demonstrated that CPT-mediated M1 reprogramming is regulated by the downregulation of TRAF6 via autophagy-dependent pathway in M2 macrophages. Study also revealed that autophagy blockade via bafilomycin A1 and si-ATG5 inhibited TRAF6 reduction and underwent auto-ubiquitination in CPT-treated M2 macrophages, suggest-

ing that CPT triggers TRAF6 autophagic degradation in lysosomes in addition to the conventional proteasomal-related pathway. In contrast to the effect of CPT in M2 macrophages, the amount of TRAF 6 was increased in M1 cells.

In inflammatory responses, ROS-dependent activation of TRAF6 forms a complex with ASK1<sup>39</sup> and induces the formation of the TAK1-TAB complex,<sup>52</sup> activating proinflammatory cytokine production. Consistent with those observations, we identified an interaction between ASK1 and TRAF6 in M1 macrophages, but not in the M2



(legend on next page)

condition (Figures 7E and 7F). Furthermore, ASK1 was decreased and ubiquitinated only in CPT-treated M1 macrophages (Figure 7G). As an ubiquitin E3 ligase, we suppose that TRAF6 participates in ASK1 ubiquitination. These results indicate that CPT induces TRAF6-mediated ASK1 degradation in M1 cells, whereas in M2 macrophages, CPT-induced TRAF6 underwent autophagic degradation and separated from ASK1. Thus, ASK1 accumulated in a dose-dependent manner in response to CPT treatment. We suggest that TRAF6 ubiquitination by CPT releases ASK1 from the complex form, enabling ASK1 to translocate to mitochondria then promote anaerobic glycolysis and superoxide production. In addition, it was found that production of proinflammatory stimuli particularly results in ASK1 and TRAF6 activation in macrophages,<sup>35,39</sup> which is consistent with our observation that ASK1 and TRAF6 highly expressed in M1 but not M2 macrophages. In M1 macrophages, TRAF6 level increased and bound to ASK1; however, the axis in M2 macrophages ran counter to M1 cells. TRAF6 acts as a rheostat to stimulate or inhibit autophagy.<sup>53</sup> In CPT-treated TAMs, we revealed a positive feedback loop in TRAF6-ASK1 axis-mediated autophagy. Following autophagy induction, TRAF6 is degraded by the autophagy lysosome and releases ASK1, which can further induce autophagy in CPT-treated TAM resembling classical activation of macrophages into M1 phenotype. Finally, we identified that CPT reverses the TRAF6-ASK1 axis in M1 and M2 macrophages.

In summary, our study clearly shows that CPT, by virtue of its ability to markedly increase glycolysis, resets TAMs from the M2 to the M1 phenotype, so the antitumor activity of CPT is due to its immunomodulatory properties. We propose that CPT has emerged as a potential immunomodulator and represents a new therapeutic avenue for cancer immunotherapy.

## MATERIALS AND METHODS

### Mice

Female NOD/SCID (NOD CB17-Prkdcscid/NcrCrl, 6 weeks of age) mice were obtained from BioLASCO Taiwan Co., Ltd. All experiments were conducted under approval granted by the Institutional Animal Care and Use Committee of China Medical University (Taichung, Taiwan) (2017-077). During the entire maintenance period, all mice were permitted free cage activity without joint immobilization. The initial body weights of the mice were between 20 and 25 g. Briefly,  $1 \times 10^6$  MDA-MB-231 cells suspended in 0.2 mL DMEM were injected individually into contralateral mammary fat pads of mice under anesthesia with isoflurane. To study the role of

macrophages in tumorigenesis, macrophages were removed from each mouse after administering clodronate liposome via a single intraperitoneal (i.p.) injection 2 days before the implantation of cancer cells (0.1 mL/10 g, Clodronate Liposomes, the Netherlands), followed by i.p. clodronate liposome injections every 4 days at the same dosage. CPT was diluted in dimethyl sulfoxide (DMSO), ethanol, normal saline, and 2-hydroxypropyl- $\beta$ -cyclodextrin (HP- $\beta$ -CD) at a ratio of 1:3:3:3 and heated to 60°C before injection. Seven days after the injection of MDA-MB-231 cells, i.p. injection with CPT was performed every other day followed by euthanization on day 30 of tumor cell inoculation. The tumors were removed, weighed, and fixed for immunohistochemical experiments. Five mice were included in each group and the results are representative of three independent experiments.

### Materials

CPT (C5624), LPS, MitoTracker Green FM (M7514), and bafilomycin A1 were purchased from Sigma-Aldrich (St. Louis, MO, USA). The fluorescein isothiocyanate-conjugated secondary antibodies were obtained from Invitrogen (Thermo Fisher Scientific, Waltham, MA, USA) and murine recombinant proteins macrophage colony stimulating factor (M-CSF), IFN- $\gamma$ , and IL-4 were purchased from Peprotech (NJ, USA).

### Cell culture and differentiation

The murine macrophage cell line RAW 264.7 and TNBC cell line MDA-MB-231 were grown in DMEM supplemented with 10% fetal bovine serum (FBS) and 100 U/mL penicillin and 100  $\mu$ g/mL streptomycin (HyClone, USA) at 37°C in a 5% CO<sub>2</sub> incubator. BMDMs collected from femurs and tibias of 6- to 8-week-old C57Bl/6 wild-type mice were cultured with RPMI-1640 Complete Medium supplemented with 10% FBS, 1% penicillin-streptomycin, and 2 mM L-glutamine in the presence of 15% L929-conditioned medium for 7 days, to allow differentiation of monocytes into macrophages. Macrophages were cultured in RPMI-1640 Complete Medium in the presence of IFN- $\gamma$  (10 ng/mL) plus 10 ng/mL LPS (Sigma-Aldrich) to induce polarization to M1 macrophages; while macrophages were exposed to IL-4 (20 ng/mL) to program to M2 macrophages.

### Cytotoxicity assay

A Cell Counting Kit-8 (CCK-8) was obtained from Dojindo (Dojindo Co. Ltd., Kumamoto, Japan). Briefly, cells were plated in 96-well plates at a density of  $1 \times 10^4$  cells per well and cultured in the growth medium. At the indicated time points, the number of cells in triplicate

### Figure 6. Induction of autophagy is ASK1-dependent

(A) Immunoblot analysis of ASK1 and TAB1/2/3 expression in CPT-treated BMDMs, as indicated. (B) RAW 264.7 cells and BMDMs were treated as indicated; lysates were examined for ASK1 expression. (C) RAW 264.7 cells and BMDMs were treated as indicated with or without 20  $\mu$ M CPT for the indicated time intervals. Total lysates were immunoblotted for ASK1 expression. (D) Immunoblot analysis of ASK1 in cytoplasmic and mitochondrial fractions of BMDM-M2 cells treated with 20  $\mu$ M CPT for the indicated time intervals. (E) Silencing of ASK1 attenuated LC3B and P62 expression in CPT-treated M2-BMDMs. RNA interference against ASK1 was conducted for M2-BMDMs treated with 20  $\mu$ M CPT for 24 h. CPT-induced increases in LC3B and P62 expression was attenuated upon ASK1 suppression. NQD1-treated (F) and ASK1 siRNA (G) M2-RAW 264.7 cells were quantified with or without CPT treatment (n = 3). Suppression of ASK1 expression significantly blocked CPT-induced changes in OCR expression. This result was supported by observations of the cytokine expression profile in RAW 264.7 cells and BMDMs (H). The results are expressed as the mean  $\pm$  SD from three independent experiments. \*\*p < 0.01 compared with controls.

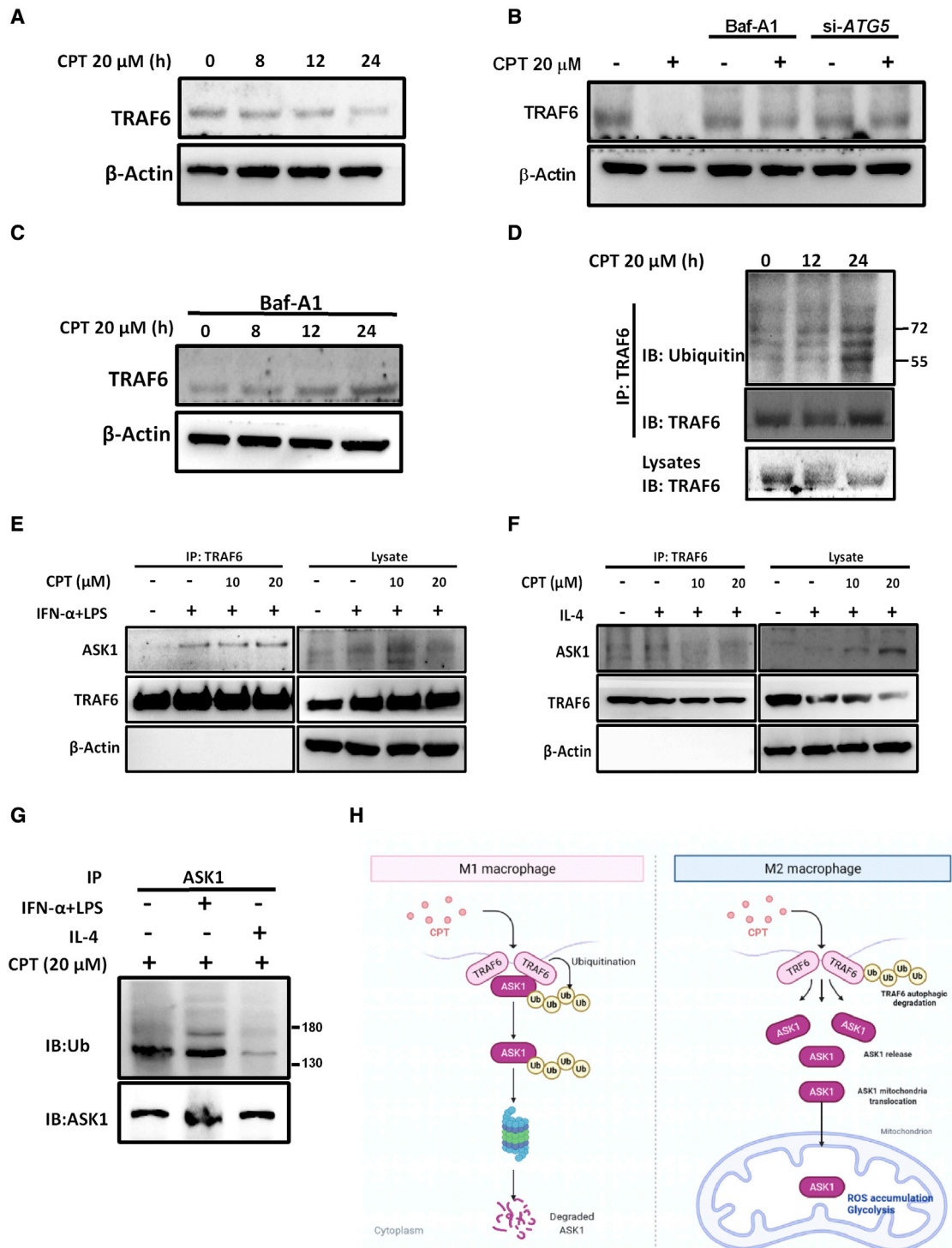


**Figure 7. Autophagy-induced TRAF6 degradation was associated with the activation of ASK1 in CPT-treated TAMs**

(A) Reduced expression of TRAF6 in CPT-treated TAMs was associated with autophagy induction. TRAF6 expression in BMDM-TAMs treated with CPT at the indicated time points was analyzed by western blotting. (B) CPT-induced suppression of TRAF6 expression appeared to be blocked when autophagy was blocked by either bafilomycin A1 or ATG5 siRNA in BMDM-TAMs. (C) Bafilomycin A1 reversed CPT-induced downregulation of TRAF6 expression. CPT-treated BMDM-TAMs were analyzed in the presence of bafilomycin A1 for TRAF6 expression at the indicated times. (D) CPT treatment induced TRAF6 auto-ubiquitination. TAMs were treated and a co-immunoprecipitation

(legend continued on next page)

wells was measured by using the absorbance at 460 nm of WST-8 formazan product. An Annexin V Apoptosis Detection Kit (640,930) was purchased from BioLegend (CA, USA). To determine whether CPT could induce cell death, cells were treated with CPT 20  $\mu$ M for 24 h or 48 h.

#### Generation of TAMs and the Transwell co-culture assay

TAMs were generated with breast tumor cell culture supernatant (TSN). Isolated BMDMs were subjected to RPMI-1640 Complete Medium containing 30% TSN for 7 days to allow differentiation to TAMs. A cell co-culture environment was established using Transwell inserts fitted with polycarbonate filters (membrane pore size, 0.4  $\mu$ m) (Corning Inc., NY, USA). Briefly, pretreated TAMs were seeded into culture inserts at the top of the Transwell filter, and MDA-MB-231 cells were seeded at the bottom well of the Boyden Chamber for 24 h. TAMs and tumor cells were kept completely separate. The inserts were then removed and tumor cells were subjected to further analysis.

#### RNA interference

All RNAi analysis was performed using ON-TARGET<sup>plus</sup> SMARTpool small interfering RNAs (siRNAs) (Dharmacon, CO, USA). Macrophage cells were seeded overnight on 6-well plates at a density of 50% confluence in medium without antibiotics, supplemented with 1% FBS. After one night of incubation, the cells were replaced with medium containing pre-mixed siRNA and TransIT-2020 Transfection Reagent (Mirus Bio, WI, USA), based on the manufacturer's instructions. Transfection efficiency was assessed by immunoblot monitoring of the expression of ASK1 in transfected cells.

#### Mitochondria staining

In order to measure transitions in mitochondrial morphology, CPT-treated cells were reacted with 100 nM MitoTracker Green FM (Invitrogen, MA, USA) for 20 min at 37°C, according to the manufacturer's instructions. After undergoing two washes in cold PBS, live cells were visualized under a Leica confocal laser scanning microscope (TCS SP8; Wetzlar, Germany). MitoTracker Green FM was monitored at an excitation wavelength of 490 nm to locate mitochondria. Fragmented mitochondria were short, punctate, and sometimes spherical, whereas filamentous mitochondria exhibited long thread-like tubular structures.

#### Flow cytometry analysis

Cells were detached and washed with cold PBS, then incubated with anti-mouse CD11b, CD115, CD80, CD86, or CD206 antibody for 15 min. Unspecific isotypes were used as controls. Cell viability was assessed by an Annexin V-FITC/7-AAD Apoptosis Detection Kit, according to the manufacturer's protocol (BioLegend, CA, USA).

Stained cells were washed and analyzed by flow cytometry (BD Canto, San Jose, CA).

#### Quantitative real-time PCR

Total RNA was extracted with a GENEzol TriRNA Pure Kit (Geneaid, New Taipei City, Taiwan). A reverse-transcription reaction was conducted with the PrimeScript RT Reagent kit (Takara, Shiga, Japan). Quantitative real-time PCR was performed with the SYBR Green Master Mix (Bio-Rad) and 1  $\mu$ M of primers using StepOne Real-Time PCR Systems (Thermo Fisher Scientific). Primer pair sequence details are supplied in Table S1, with *GAPDH* serving as the internal control. Relative expression levels of target genes against *GAPDH* are expressed as  $2^{-\Delta Ct}$  and fold differences in total counts are calculated as expressed mRNA of CPT-treated samples compared with untreated samples.

#### Immunoblotting

CPT-treated cells were harvested and total cell protein was extracted using whole-cell lysis buffer. Protein concentrations were determined by the Bradford method (Bio-Rad). Samples with equal amounts of protein were subjected to 8% to 15% SDS-PAGE and transferred onto a polyvinylidene difluoride (PVDF) membrane (Millipore). The membrane was incubated at room temperature in blocking buffer (5% BSA) for 1 h, then incubated overnight in blocking solution containing an appropriate dilution of anti-STAT3, phosphorylated STAT3 (p-STAT3), STAT6, p-STAT6, TRAF6, LC3B, ATG5, p-JNK, JNK, p-mTOR, ubiquitin (Cell Signaling), apoptosis signal-regulating kinase 1 (ASK1) (Abcam), TAB1, TAB2, TAB3 (Santa Cruz Biotechnology, Inc.), and  $\beta$ -actin antibody (Elabscience). After washing, blots were probed with the appropriate secondary horseradish peroxidase-conjugated secondary antibodies (Jackson ImmunoResearch), detected by the enhanced chemiluminescence detection system (Millipore) and scanned by the ChemiDoc XRS + System (Bio-Rad).  $\beta$ -Actin served as the internal control. Cytosolic and mitochondrial protein extractions were performed according to the manufacturer's protocol (Thermo Scientific). HSP60 and  $\alpha$ -tubulin were used as mitochondrial and cytosolic markers, respectively.

#### Co-IP assay

The co-IP assay was performed using protein G Mag Sepharose Xtra magnetic (Cytiva), according to the manufacturer's instructions. Briefly, the cell proteins were extracted with Pierce IP Lysis Buffer (Thermo Fisher Scientific) supplemented with PhosSTOP proteinase inhibitor and complete phosphatase inhibitor cocktails (Roche, Basel, Switzerland). The target protein was precipitated through binding with target antibody using prebound magnetic beads and eluted by PBS supplemented with 0.1% Tween 20. Isolated protein was further

---

assay was conducted. Increased association of TRAF6 with ubiquitin was observed in CPT-treated TAMs. Reduced TRAF6 expression was also observed in total cell lysate. (E and F) M1 and M2 RAW 264.7 cells were treated with CPT at the indicated doses for 24 h and a co-immunoprecipitation assay was conducted. Increased association of TRAF6 with ASK1 was observed in CPT-treated M1 cells. (G) CPT treatment induced ASK1 ubiquitination in M1-RAW 264.7 cells. M1 and M2 cells were treated and a co-immunoprecipitation assay was conducted. Increased association of ASK1 with ubiquitin was observed in CPT-treated M1 cells. (H) Schematic diagram of the mechanism underlying degradation of ASK1 in M1 macrophages (left) and repolarization of CPT-treated TAMs to the M1 phenotype (right).

denatured by heating at 95°C with sample buffer. The targeted protein and other interacted proteins were separated using SDS-PAGE and protein expression levels were quantified. The input lysates served as the loading controls of the targeted proteins.

#### Macrophage function and NO measurement

Culture supernatants of untreated and CPT-treated macrophages were collected after 48 h. IL-6, IL-1 $\beta$ , IL-10, and TNF- $\alpha$  were quantified by ELISA in accordance with the supplier's protocols (Invitrogen). The Griess Reagent System was used to measure NO production in CPT-treated cells, according to the manufacturer's instructions (Abcam).

#### RNA sequencing

Total RNA in each sample was extracted using the TRIzol Reagent (Invitrogen)/RNeasy Mini Kit (Qiagen), then quantified and qualified using Agilent 2100 Bioanalyzer (Agilent Technologies, Palo Alto, CA, USA), NanoDrop (Thermo Fisher Scientific Inc.) and 1% agarose gel; 1  $\mu$ g total RNA with RIN value above 6.5 was used for preparing the next-generation sequencing library, following the manufacturer's protocol. Poly (A) mRNA isolation was performed using the Poly(A) mRNA Magnetic Isolation Module or the rRNA Removal Kit. mRNA fragmentation and priming were performed using First Strand Synthesis Reaction Buffer and Random Primers. First-strand cDNA was synthesized using ProtoScript II Reverse Transcriptase, while second-strand cDNA was synthesized using Second Strand Synthesis Enzyme Mix. Double-stranded cDNA was purified using beads, then treated with End Prep Enzyme Mix to repair both ends and add dA tailing in one reaction, followed by a T-A ligation to add adaptors to both ends. Size selection of adaptor-ligated DNA was then performed using beads, and fragments of ~420 base pairs (bp) (with the approximate insert size of 300 bp) were recovered. Each sample underwent PCR amplification for 13 cycles using the P5 and P7 primers, both of which contain sequences that anneal to the flow cells and generate bridge PCR, while the P7 primers also carry a six-base index that allows for multiplexing. The PCR products were cleaned up using beads, validated using a Qsep100 (Bioptic, Taiwan), then quantified using the Qubit 3.0 Fluorometer (Invitrogen, Carlsbad, CA, USA). Libraries with different indices were multiplexed and loaded onto an Illumina HiSeq instrument, following the manufacturer's instructions (Illumina, San Diego, CA, USA). Sequencing was carried out using a 2  $\times$  150-bp paired-end configuration; image analysis and base calling were conducted using HiSeq Control Software (HCS) + OLB + GAPipeline-1.6 (Illumina) on the HiSeq instrument. The sequences were processed and analyzed by GENEWIZ.

#### Histological examination

The tumor mass dissected from mice was weighed and fixed in 4% paraformaldehyde (pH 7.5) for 4 h and then processed for paraffin embedding according to standard histological procedures. Sections with thickness of 4  $\mu$ m were prepared and stained with H&E. The paraffin-embedded sample slides were de-paraffinized, hydrated, and then stained with hematoxylin for 1 min. After rinse, the slides were stained with eosin for 5 min, rinsed, and sealed with cover slips.

The slides were counterstained with hematoxylin and mounted. All slides were examined under light microscopy.

#### Statistical analysis

All experiments were performed in triplicate and all data represent the mean  $\pm$  SD of three individual experiments. Statistical analyses were performed using GraphPad Prism software (version 6, GraphPad Software, Inc., San Diego, CA, USA). One-way ANOVA was applied when evaluating significant values of multiple comparisons. A *p* value of less than 0.05 was considered to be significant.

#### DATA AVAILABILITY

All raw data are available upon request.

#### SUPPLEMENTAL INFORMATION

Supplemental information can be found online at <https://doi.org/10.1016/j.omto.2022.06.008>.

#### ACKNOWLEDGMENTS

The authors thank Iona J. MacDonald from China Medical University, Taichung, Taiwan, for her critical reading and revision of our manuscript. This work was supported and funded by the Ministry of Science and Technology of Taiwan [MOST 110-2320-B-039-40-], China Medical University Hospital [DMR-110-189, DMR-111-005, DMR-111-013, DMR-111-016, and DMR-111-195], and An-Nan Hospital, China Medical University [ANHRF-110-25].

#### AUTHOR CONTRIBUTIONS

J.H.Y. wrote the original draft, participated in the design of the study, and performed the experiments. W.C.H. performed the experiments, data collection, and interpretation. S.C.L., Y.I.H., and W.T.C. performed the experiments and analyzed the data. G.J.T. and M.C.H. provided resources, administration supports, and data amendment. S.T.H. designed, conceived the study, interpret the data, and wrote the manuscript. All authors read and approved the final manuscript.

#### DECLARATION OF INTERESTS

The authors declare no competing interests.

#### REFERENCES

- De Henau, O., Rausch, M., Winkler, D., Campesato, L.F., Liu, C., Cymerman, D.H., Budhu, S., Ghosh, A., Pink, M., Tchaicha, J., et al. (2016). Overcoming resistance to checkpoint blockade therapy by targeting PI3K $\gamma$  in myeloid cells. *Nature* 539, 443–447. <https://doi.org/10.1038/nature20554>.
- Guerrero, J.L., Sotayo, A., Ponichtera, H.E., Castrillon, J.A., Pourzia, A.L., Schad, S., Johnson, S.F., Carrasco, R.D., Lazo, S., Bronson, R.T., et al. (2017). Class IIa HDAC inhibition reduces breast tumours and metastases through anti-tumour macrophages. *Nature* 543, 428–432. <https://doi.org/10.1038/nature21409>.
- Mantovani, A., Marchesi, F., Malesci, A., Laghi, L., and Allavena, P. (2017). Tumour-associated macrophages as treatment targets in oncology. *Nat. Rev. Clin. Oncol.* 14, 399–416. <https://doi.org/10.1038/nrclinonc.2016.217>.
- Lin, Y., Xu, J., and Lan, H. (2019). Tumor-associated macrophages in tumor metastasis: biological roles and clinical therapeutic applications. *J. Hematol. Oncol.* 12, 76. <https://doi.org/10.1186/s13045-019-0760-3>.
- Wang, Y., Guo, G., Feng, Y., Long, H., Ma, D.L., Leung, C.H., Dong, L., and Wang, C. (2017). A tumour microenvironment-responsive polymeric complex for targeted

- depletion of tumour-associated macrophages (TAMs). *J. Mater. Chem. B* 5, 7307–7318. <https://doi.org/10.1039/c7tb01495c>.
6. Orillion, A., Damayanti, N.P., Shen, L., Adelaiye-Ogala, R., Affronti, H., Elbanna, M., Chintala, S., Ciesielski, M., Fontana, L., Kao, C., et al. (2018). Dietary protein restriction reprograms tumor-associated macrophages and enhances immunotherapy. *Clin. Cancer Res.* 24, 6383–6395. <https://doi.org/10.1158/1078-0432.ccr-18-0980>.
  7. Biswas, S.K., and Mantovani, A. (2010). Macrophage plasticity and interaction with lymphocyte subsets: cancer as a paradigm. *Nat. Immunol.* 11, 889–896. <https://doi.org/10.1038/ni.1937>.
  8. Yang, Q., Guo, N., Zhou, Y., Chen, J., Wei, Q., and Han, M. (2020). The role of tumor-associated macrophages (TAMs) in tumor progression and relevant advance in targeted therapy. *Acta Pharm. Sin. B* 10, 2156–2170. <https://doi.org/10.1016/j.apsb.2020.04.004>.
  9. Lu, B., and Finn, O.J. (2008). T-cell death and cancer immune tolerance. *Cell Death Differ.* 15, 70–79. <https://doi.org/10.1038/sj.cdd.4402274>.
  10. Mapara, M.Y., and Sykes, M. (2004). Tolerance and cancer: mechanisms of tumor evasion and strategies for breaking tolerance. *J. Clin. Oncol.* 22, 1136–1151. <https://doi.org/10.1200/jco.2004.10.041>.
  11. Diskin, B., Adam, S., Cassini, M.F., Sanchez, G., Liria, M., Aykut, B., Buttar, C., Li, E., Sundberg, B., Salas, R.D., et al. (2020). PD-L1 engagement on T cells promotes self-tolerance and suppression of neighboring macrophages and effector T cells in cancer. *Nat. Immunol.* 21, 442–454. <https://doi.org/10.1038/s41590-020-0620-x>.
  12. Seidel, J.A., Otsuka, A., and Kabashima, K. (2018). Anti-PD-1 and anti-CTLA-4 therapies in cancer: mechanisms of action, efficacy, and limitations. *Front. Oncol.* 8, 86. <https://doi.org/10.3389/fonc.2018.00086>.
  13. Peng, Q., Qiu, X., Zhang, Z., Zhang, S., Zhang, Y., Liang, Y., Guo, J., Peng, H., Chen, M., Fu, Y.X., and Tang, H. (2020). PD-L1 on dendritic cells attenuates T cell activation and regulates response to immune checkpoint blockade. *Nat. Commun.* 11, 4835. <https://doi.org/10.1038/s41467-020-18570-x>.
  14. Patsoukis, N., Wang, Q., Strauss, L., and Boussiotis, V.A. (2020). Revisiting the PD-1 pathway. *Sci. Adv.* 6, eabd2712. <https://doi.org/10.1126/sciadv.abd2712>.
  15. Galvan-Pena, S., and O'Neill, L.A.J. (2014). Metabolic reprogramming in macrophage polarization. *Front. Immunol.* 5, 420. <https://doi.org/10.3389/fimmu.2014.00420>.
  16. Tan, Z., Xie, N., Cui, H., Moellering, D.R., Abraham, E., Thannickal, V.J., and Liu, G. (2015). Pyruvate dehydrogenase kinase 1 participates in macrophage polarization via regulating glucose metabolism. *J. Immunol.* 194, 6082–6089. <https://doi.org/10.4049/jimmunol.1402469>.
  17. Cramer, T., Yamanishi, Y., Clausen, B.E., Förster, I., Pawlinski, R., Mackman, N., Haase, V.H., Jaenisch, R., Corr, M., Nizet, V., et al. (2003). HIF-1 $\alpha$  is essential for myeloid cell-mediated inflammation. *Cell* 112, 645–657. [https://doi.org/10.1016/s0092-8674\(03\)00154-5](https://doi.org/10.1016/s0092-8674(03)00154-5).
  18. Shin, D.S., Kim, H.N., Shin, K.D., Yoon, Y.J., Kim, S.J., Han, D.C., and Kwon, B.M. (2009). Cryptotanshinone inhibits constitutive signal transducer and activator of transcription 3 function through blocking the dimerization in DU145 prostate cancer cells. *Cancer Res.* 69, 193–202. <https://doi.org/10.1158/0008-5472.can-08-2575>.
  19. Ahmad, Z., Ng, C.T., Fong, L.Y., Bakar, N.A.A., Hussain, N.H.M., Ang, K.P., Ee, G.C.L., and Hakim, M.N. (2016). Cryptotanshinone inhibits TNF- $\alpha$ -induced early atherogenic events in vitro. *J. Physiol. Sci.* 66, 213–220. <https://doi.org/10.1007/s12576-015-0410-7>.
  20. Tang, S., Shen, X.Y., Huang, H.Q., Xu, S.W., Yu, Y., Zhou, C.H., Chen, S.R., Le, K., Wang, Y.H., and Liu, P.Q. (2011). Cryptotanshinone suppressed inflammatory cytokines secretion in RAW264.7 macrophages through inhibition of the NF- $\kappa$ B and MAPK signaling pathways. *Inflammation* 34, 111–118. <https://doi.org/10.1007/s10753-010-9214-3>.
  21. Zhang, F., Zheng, W., Pi, R., Mei, Z., Bao, Y., Gao, J., Tang, W., Chen, S., and Liu, P. (2009). Cryptotanshinone protects primary rat cortical neurons from glutamate-induced neurotoxicity via the activation of the phosphatidylinositol 3-kinase/Akt signaling pathway. *Exp. Brain Res.* 193, 109–118. <https://doi.org/10.1007/s00221-008-1600-9>.
  22. Chen, L., Zheng, S.Z., Sun, Z.G., Wang, A.Y., Huang, C.H., Puchard, N.A., Huang, S.L., Gao, X., and Lu, Y. (2011). Cryptotanshinone has diverse effects on cell cycle events in melanoma cell lines with different metastatic capacity. *Cancer Chemother. Pharmacol.* 68, 17–27. <https://doi.org/10.1007/s00280-010-1440-8>.
  23. Chen, W., Luo, Y., Liu, L., Zhou, H., Xu, B., Han, X., Shen, T., Liu, Z., Lu, Y., and Huang, S. (2010). Cryptotanshinone inhibits cancer cell proliferation by suppressing Mammalian target of rapamycin-mediated cyclin D1 expression and Rb phosphorylation. *Cancer Prev. Res.* 3, 1015–1025. <https://doi.org/10.1158/1940-6207.capr-10-0020>.
  24. Park, I.J., Kim, M.J., Park, O.J., Park, M.G., Choe, W., Kang, I., Kim, S.S., and Ha, J. (2010). Cryptotanshinone sensitizes DU145 prostate cancer cells to Fas(APO1/CD95)-mediated apoptosis through Bcl-2 and MAPK regulation. *Cancer Lett.* 298, 88–98. <https://doi.org/10.1016/j.canlet.2010.06.006>.
  25. Tse, A.K.W., Chow, K.Y., Cao, H.H., Cheng, C.Y., Kwan, H.Y., Yu, H., Zhu, G.Y., Wu, Y.C., Fong, W.F., and Yu, Z.L. (2013). The herbal compound cryptotanshinone restores sensitivity in cancer cells that are resistant to the tumor necrosis factor-related apoptosis-inducing ligand. *J. Biol. Chem.* 288, 29923–29933. <https://doi.org/10.1074/jbc.m113.483909>.
  26. Yuan, D.P., Long, J., Lu, Y., Lin, J., and Tong, L. (2014). The forecast of anticancer targets of cryptotanshinone based on reverse pharmacophore-based screening technology. *Chin. J. Nat. Med.* 12, 443–448. [https://doi.org/10.1016/s1875-5364\(14\)60069-8](https://doi.org/10.1016/s1875-5364(14)60069-8).
  27. Yen, J.H., Huang, H.S., Chuang, C.J., and Huang, S.T. (2019). Activation of dynamin-related protein 1 - dependent mitochondria fragmentation and suppression of osteosarcoma by cryptotanshinone. *J. Exp. Clin. Cancer Res.* 38, 42. <https://doi.org/10.1186/s13046-018-1008-8>.
  28. Tavares, A.J., Poon, W., Zhang, Y.N., Dai, Q., Besla, R., Ding, D., Ouyang, B., Li, A., Chen, J., Zheng, G., et al. (2017). Effect of removing Kupffer cells on nanoparticle tumor delivery. *Proc. Natl. Acad. Sci. USA* 114, E10871–E10880. <https://doi.org/10.1073/pnas.1713390114>.
  29. Huang, S.C.C., Everts, B., Ivanova, Y., O'Sullivan, D., Nascimento, M., Smith, A.M., Beatty, W., Love-Gregory, L., Lam, W.Y., O'Neill, C.M., et al. (2014). Cell-intrinsic lysosomal lipolysis is essential for alternative activation of macrophages. *Nat. Immunol.* 15, 846–855. <https://doi.org/10.1038/ni.2956>.
  30. Pearce, E.L., and Pearce, E.J. (2013). Metabolic pathways in immune cell activation and quiescence. *Immunity* 38, 633–643. <https://doi.org/10.1016/j.immuni.2013.04.005>.
  31. Nomura, M., Liu, J., Rovira, I.L., Gonzalez-Hurtado, E., Lee, J., Wolfgang, M.J., and Finkel, T. (2016). Fatty acid oxidation in macrophage polarization. *Nat. Immunol.* 17, 216–217. <https://doi.org/10.1038/ni.3366>.
  32. Murray, P.J., Allen, J.E., Biswas, S.K., Fisher, E.A., Gilroy, D.W., Goerdt, S., Gordon, S., Hamilton, J.A., Ivashkiv, L.B., Lawrence, T., et al. (2014). Macrophage activation and polarization: nomenclature and experimental guidelines. *Immunity* 41, 339–340. <https://doi.org/10.1016/j.immuni.2014.07.009>.
  33. Sica, A., and Mantovani, A. (2012). Macrophage plasticity and polarization: in vivo veritas. *J. Clin. Invest.* 122, 787–795. <https://doi.org/10.1172/jci59643>.
  34. You, L., Wang, Z., Li, H., Shou, J., Jing, Z., Xie, J., Sui, X., Pan, H., and Han, W. (2015). The role of STAT3 in autophagy. *Autophagy* 11, 729–739. <https://doi.org/10.1080/15548627.2015.1017192>.
  35. Hayakawa, R., Hayakawa, T., Takeda, K., and Ichijo, H. (2012). Therapeutic targets in the ASK1-dependent stress signaling pathways. *Proc. Jpn. Acad. Ser. B, Phys. Biol. Sci.* 88, 434–453. <https://doi.org/10.2183/pjab.88.434>.
  36. Liu, H., Nishitoh, H., Ichijo, H., and Kyriakis, J.M. (2000). Activation of apoptosis signal-regulating kinase 1 (ASK1) by tumor necrosis factor receptor-associated factor 2 requires prior dissociation of the ASK1 inhibitor thioredoxin. *Mol. Cell Biol.* 20, 2198–2208. <https://doi.org/10.1128/mcb.20.6.2198-2208.2000>.
  37. Zhang, R., Al-Lamki, R., Bai, L., Streb, J.W., Miano, J.M., Bradley, J., and Min, W. (2004). Thioredoxin-2 inhibits mitochondria-located ASK1-mediated apoptosis in a JNK-independent manner. *Circ. Res.* 94, 1483–1491. <https://doi.org/10.1161/01.res.0000130525.37646.a7>.
  38. Ji, Y.X., Zhang, P., Zhang, X.J., Zhao, Y.C., Deng, K.Q., Jiang, X., Wang, P.X., Huang, Z., and Li, H. (2016). The ubiquitin E3 ligase TRAF6 exacerbates pathological cardiac hypertrophy via TAK1-dependent signalling. *Nat. Commun.* 7, 11267. <https://doi.org/10.1038/ncomms11267>.
  39. Matsuzawa, A., Saegusa, K., Noguchi, T., Sadamitsu, C., Nishitoh, H., Nagai, S., Koyasu, S., Matsumoto, K., Takeda, K., and Ichijo, H. (2005). ROS-dependent

- activation of the TRAF6-ASK1-p38 pathway is selectively required for TLR4-mediated innate immunity. *Nat. Immunol.* 6, 587–592. <https://doi.org/10.1038/ni1200>.
40. Bardia, A., Hurvitz, S.A., Tolaney, S.M., Loirat, D., Punie, K., Oliveira, M., Brufsky, A., Sardesai, S.D., Kalinsky, K., Zelnak, A.B., et al. (2021). Sacituzumab govitecan in metastatic triple-negative breast cancer. *New Engl. J. Med.* 384, 1529–1541. <https://doi.org/10.1056/nejmoa2028485>.
  41. Cao, X., Li, B., Chen, J., Dang, J., Chen, S., Gunes, E.G., Xu, B., Tian, L., Muend, S., Raoof, M., et al. (2021). Effect of cabazitaxel on macrophages improves CD47-targeted immunotherapy for triple-negative breast cancer. *J. Immunother. Cancer* 9, e002022. <https://doi.org/10.1136/jitc-2020-002022>.
  42. Ma, Y., Mattarollo, S.R., Adjemian, S., Yang, H., Aymeric, L., Hannani, D., Portela Catani, J.P., Duret, H., Teng, M.W., Kepp, O., et al. (2014). CCL2/CCR2-dependent recruitment of functional antigen-presenting cells into tumors upon chemotherapy. *Cancer Res.* 74, 436–445. <https://doi.org/10.1158/0008-5472.can-13-1265>.
  43. O'Neill, L.A., and Pearce, E.J. (2016). Immunometabolism governs dendritic cell and macrophage function. *J. Exp. Med.* 213, 15–23. <https://doi.org/10.1084/jem.20151570>.
  44. Allavena, P., Sica, A., Garlanda, C., and Mantovani, A. (2008). The Yin-Yang of tumor-associated macrophages in neoplastic progression and immune surveillance. *Immunol. Rev.* 222, 155–161. <https://doi.org/10.1111/j.1600-065x.2008.00607.x>.
  45. Shields, C.W., Evans, M.A., Wang, L.L.W., Wang, L.L., Baugh, N., Iyer, S., Wu, D., Zhao, Z., Pusuluri, A., Ukidve, A., et al. (2020). Cellular backpacks for macrophage immunotherapy. *Sci. Adv.* 6, eaaz6579. <https://doi.org/10.1126/sciadv.aaz6579>.
  46. Chang, H.Y., Nishitoh, H., Yang, X., Ichijo, H., and Baltimore, D. (1998). Activation of apoptosis signal-regulating kinase 1 (ASK1) by the adapter protein Daxx. *Science* 281, 1860–1863. <https://doi.org/10.1126/science.281.5384.1860>.
  47. Ichijo, H., Nishida, E., Irie, K., Dijke, P.T., Saitoh, M., Moriguchi, T., Takagi, M., Matsumoto, K., Miyazono, K., and Gotoh, Y. (1997). Induction of apoptosis by ASK1, a mammalian MAPKKK that activates SAPK/JNK and p38 signaling pathways. *Science* 275, 90–94. <https://doi.org/10.1126/science.275.5296.90>.
  48. Mochida, Y., Takeda, K., Saitoh, M., Nishitoh, H., Amagasa, T., Ninomiya-Tsuji, J., Matsumoto, K., and Ichijo, H. (2000). ASK1 inhibits interleukin-1-induced NF-kappa B activity through disruption of TRAF6-TAK1 interaction. *J. Biol. Chem.* 275, 32747–32752. <https://doi.org/10.1074/jbc.m003042200>.
  49. Osaka, N., Takahashi, T., Murakami, S., Matsuzawa, A., Noguchi, T., Fujiwara, T., Aburatani, H., Moriyama, K., Takeda, K., and Ichijo, H. (2007). ASK1-dependent recruitment and activation of macrophages induce hair growth in skin wounds. *J. Cell Biol.* 176, 903–909. <https://doi.org/10.1083/jcb.200611015>.
  50. Zhao, Q., Liu, Y., Zhong, J., Bi, Y., Liu, Y., Ren, Z., Li, X., Jia, J., Yu, M., and Yu, X. (2019). Pristimerin induces apoptosis and autophagy via activation of ROS/ASK1/JNK pathway in human breast cancer in vitro and in vivo. *Cell Death Discov.* 5, 125. <https://doi.org/10.1038/s41420-019-0208-0>.
  51. Chen, P., Cescon, M., and Bonaldo, P. (2014). Autophagy-mediated regulation of macrophages and its applications for cancer. *Autophagy* 10, 192–200. <https://doi.org/10.4161/auto.26927>.
  52. Ajibade, A.A., Wang, H.Y., and Wang, R.F. (2013). Cell type-specific function of TAK1 in innate immune signaling. *Trends Immunol.* 34, 307–316. <https://doi.org/10.1016/j.it.2013.03.007>.
  53. Shi, C.S., and Kehrl, J.H. (2010). TRAF6 and A20 regulate lysine 63-linked ubiquitination of Beclin-1 to control TLR4-induced autophagy. *Sci. Signal.* 3, ra42. <https://doi.org/10.1126/scisignal.2000751>.